Bima Journal of Science and Technology, Vol. 6 (3) Dec, 2022 ISSN: 2536-6041

DOI: 10.56892/bima.v6i03.47

PHOTOCATALYTIC DEGRADATION EFFICIENCY OF *Mangifera indica* MEDIATED ZINC OXIDE NANOPARTICLES

[1]*SOLOMON ALMANTO MAMURU, [1]AISHA UMAR HAROON and [2]SAMINU HAMMAN BARAU

[1]Department of Pure and Applied Chemistry, Adamawa State University, Mubi
[2]Department of Science Laboratory Technology, Adamawa State Polytechnic, Yola

Corresponding Author: mamuru19@adsu.edu.ng

ABSTRACT

The synthesis of metal nanoparticles using biological entities proven to be environmentally friendly against the physical and chemical method, the use of these metal nanoparticles as catalyst in the treatment of wastewater have also shown a lot of advantage against other techniques. In this research zinc oxide nanoparticles were successfully synthesized using aqueous leave extract of *Mangifera indica*, through a one-step synthesis protocol, results obtained from the UV-visible spectroscopy shows that the nanoparticles absorb light at 297 nm, while the scanning electron microscope reveals the morphology of the particles as flat sheet and highly agglomerated having 51.53 nm as the size from the X-ray diffraction. The FTIR spectroscopy reveals functional group of alcohol, amides, alkane, alkanes, amines, ethers Ar-O-R, alkenes, alkanes, as possible groups that may be responsible for the reduction of metal salt to metal oxide nanoparticles. The photocatalytic performance of the nanoparticles in the degradation of Congo red dye increases with increase in catalyst loading with the apparent kinetic rate constant, k_{app} as 8.8×10^{-2} min^{-1}, 6.6×10^{-2} min^{-1}, and 5.7×10^{-2} min^{-1} for 1 mg, 2 mg, and 3 mg, respectively, suggesting that the nanoparticle has potential in the degradation of Congo red dye.

Keywords: Photocatalysis; Biosynthesis; Zinc oxide nanoparticles; *Mangifera indica*; Congo red.

INTRODUCTION

Recently, metal/metal oxide nanoparticles have garnered a lot of interest. Their small particle size, large surface area, quantum confinement, and other phenomena are particularly responsible for this. They exhibit characteristics that differ greatly from those of bulk materials (Roduner, 2006) . These nanoparticles can be produced using a variety of techniques, including chemical (Lyon, Fleming, Stone, Schiffer, & Williams, 2004) and physical ones (Lu, et al., 2007) , but biological production of the particles offers advantages over less efficient and hazardous chemical and physical processes (Mamuru & Jaji, 2015).

Zinc oxide, also known by its chemical formula ZnO, is an inorganic substance that possesses catalytic, semiconducting, piezoelectric, optoelectronic, and pyroelectric properties, owing to their huge surface area to volume ratio and a wide gap between their conduction and valence bands, its nanoparticles (ZnO NPs) display unique capabilities such as greater absorption of light and enhanced catalytic properties (Ramesh, Anbuvannan, & Viruthagiri, 2015).

Without sufficient filtration, the discharge of effluents from the textile and tannery sectors can pose environmental health risks. Since these effluents are often allowed to deteriorate with the assistance of sunlight, the addition of

DOI: 10.56892/bima.v6i03.47

a catalyst will speed up the degradation process.

The goal of this study is to demonstrate the potential of biologically produced metal oxide nanoparticles as a catalyst for the breakdown of contaminated dye water.

MATERIALS AND METHODS

Preparation of Extract

The zinc oxide nanoparticles were produced by reducing the precursor salt of zinc sulphate using the aqueous leaf extracts of *Mangifera indica* due to its high availability and cost effectiveness. 10 g of *Mangifera indica* leaves were weighed and then washed with running tap water followed by deionized water. The thoroughly cleaned leaves were then place in 500 ml beaker containing 100 ml of deionized water and then heat on a hotplate at 60°C. The solution was brought to the boil for 15 minutes allowed to cool and filtered using Whatman filter paper No. 1.

Preparation of Zinc Oxide Nanoparticles

71.89 g of zinc sulphate was dissolved in 500 ml deionized water to form 0.5 M zinc sulphate solution. 100 ml of the zinc sulphate solution was placed in a conical flask, 25 ml of the leaf extract was added dropwise and stirred using magnetic stirrer for 60 minutes at 80°C and drop of sodium hydroxide was added to increase the pH of the solution. The reaction was stopped after the solution turned brown, afterward the solution was allowed to cool down then centrifuged at 3000 rpm for 30 minutes and then rinsed until neutral the precipitate was then dried in an oven under 100°C, the dried sample was pulverized as the nanoparticles then stored in a storage bottle for further analysis.

Preparation of Dye (Congo Red) Solution

1 mM of Congo red solution was prepared in 100 ml volumetric flask and used for carrying out Photocatalytic studies.

Characterization of Zinc Oxide Nanoparticles

The following microscopic and spectroscopic techniques were used to confirm the presence of the nanoparticle after the synthesis: Ultraviolet-visible spectroscopy (UV-vis.); Fourier transform infra-red spectroscopy (FTIR); Scanning electron microscopy (SEM) and X-ray diffraction (XRD).

Photocatalytic Study

5 ml of 1mM dye solution was placed into 15 different sample bottles with different weights of 1 mg, 2 mg and 3 mg of zinc oxide nanoparticles and kept under direct sunlight at different hours of 1hr, 2hrs, 3hrs, 4hrs and 5hrs for the photocatalytic studies. The change in concentration of the dye molecule after addition of zinc oxide nanoparticles was used to determine the adsorption level of dye. UV-visible spectroscopy was employed for this purpose.

RESULTS

Reaction Color and UV-visible Spectroscopy

Inset to Fig. 1 shows the change in color of the colorless zinc salt to brown of zinc oxide nanoparticles when the extract was added indicating the formation of nanoparticles (Ghidan, Al-Antary, & Awwad, 2016). The formation of ZnO NPs from zinc sulphate solution was studied using UV-visible spectroscopy because a visible color change (from yellowish to brownish) occurred, indicating the formation of nanoparticles. The intensity of the brownish color of the NPs increased as the concentration of plant extract, sodium hydroxide, and heat increased. The absorption spectra of zinc oxide nanoparticles as shown in Figure 1 is at 292 nm; the peak's sharpness indicates that the particles were pure and homogeneous in size, while the

DOI: 10.56892/bima.v6i03.47

band's narrowness indicates that the particles were mono-dispersed.

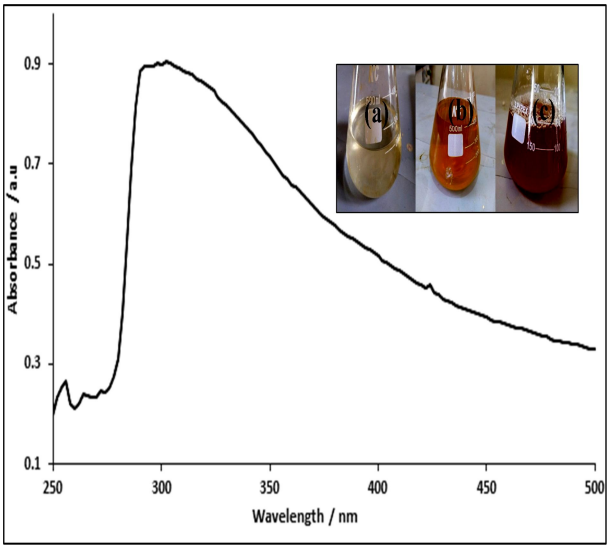

Figure 1: UV-visible spectroscopy spectrum of zinc oxide nanoparticles. (inset) color change of the synthesis, zinc sulphate solution (a), aqueous extract of *Mangifera indica* leaves (b), zinc oxide nanoparticles (c)

The band gap energy was also determined using the Planck's equation to predict the electrical conductivity of the nanoparticle.

Energy of the band gap (E) = hC/ (λ) ……. (1)

Where h = Planck's constant = 6.626 x 10^{-34} Js, C = Light speed = 3.0 x 10^{8} ms^{-1}, and λ = Cutoff wavelength = 292 x 10^{-9} meters.

The band gap energy of zinc oxide nanoparticle was calculated to be around 4.23 eV, implying that zinc oxide nanoparticle has very low electrical conductivity, as substances with high band gaps (> 4 eV) are known as insulators, as they prevent electron passage. Semiconductors have band gaps of less than 3 eV, whereas conductors have very small band gaps or none.

Fourier Transform Infra-red Spectroscopy

Fourier transform infrared spectroscopy provide evidence that functional groups are in the ZnO NPs sample. The vibrational peaks in the FTIR spectra depicted in Figure 2 were primarily found at cm^{-1} 3200.99, 1570.22, 1429.22, 1338.39, 1199.33, 1059.32, 823.94, and 750.59. Alcohol and alkenes are both indicated by the strong broad peak at 3200.99 and 823.94 cm^{-1}, respectively, which is caused by the stretching of the O-H bond and the bending of the C-H bond. The bands at 1059.32 and 750.59 cm^{-1} are caused by the existence of C-O-C symmetric stretch and C-H stretch, while the amide and amines are present at 1570.22 and 1199.33 cm^{-1} due to the CO-NH_2 and C-N stretch, and the alkane is present at 1429.22 and 1338.38 cm^{-1} due to their C-H bending. We assume that this bands show the presence of protein and hydroxyl groups in the ZnO NPs which may be responsible for the reduction of the metal salt (Ghidan, Al-Antary, & Awwad, 2016; Kumar, Mahajan, Kaur, & Kim, 2017).

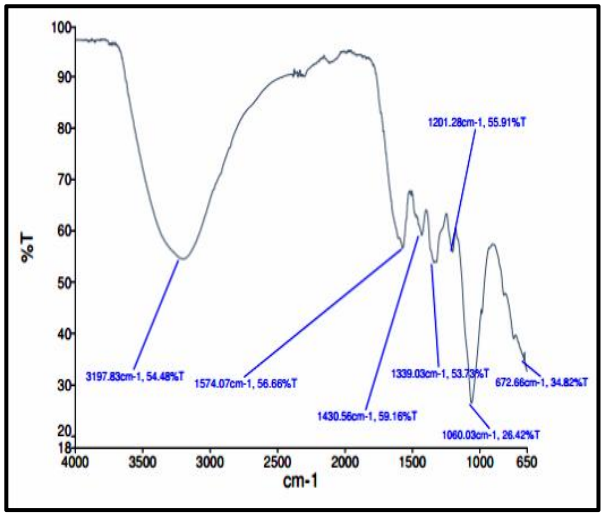

Figure 2: FTIR spectroscopy absorption spectrum of zinc oxide nanoparticle.

Scanning Electron Microscope (SEM) Analysis

The scanning electron microscope was used to explore the morphological and structural analyses of zinc oxide nanoparticles as shown in Figure 3. The nanoparticles appear as "flat

DOI: 10.56892/bima.v6i03.47

sheets" and are strongly agglomerated in SEM micrographs.

Figure 3: SEM morphology of zinc oxide nanoparticle

X-ray Diffraction (XRD)

The powder X-ray diffraction (pXRD) patterns of the produced zinc oxide nanoparticles proved their crystalline character, as shown in Figure 4. The (100), (002), and (101) planes of monoclinic ZnO are attributed to a succession of diffraction peaks at 29.26°, 34.92°, and 38.66°, respectively. The diffraction peak at 2θ = 38.66° gave the maximum intensity and was used to determine the crystallite size using the Debye Scherrer formula (Sivaraj, Rahman, Rajiv, Salam, & Venckatesh, 2014) . The crystallite size was calculated to be 51.53 nanometers.

$$D = \frac{0.9\lambda}{\beta Cos\theta} \quad \ldots\ldots\ldots\ldots\ldots\ldots\ldots\ldots (2)$$

Where, D = crystallite size, (Angstrom), λ = X-ray wavelength = 1.5418 for Cu Kα, β = FWHM (in radian) obtained from the 38.66° peak, θ = observed peak angle, degree

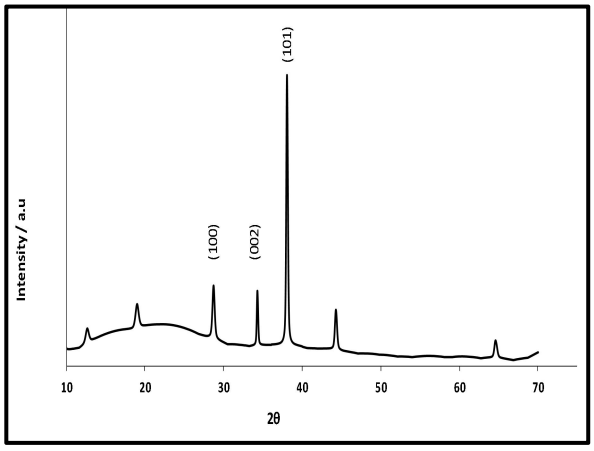

Figure 4: Powder X-ray diffraction pattern of zinc oxide nanoparticles

Photocatalytic Degradation of Congo Red Dye

The adsorption level of dye was determined by measuring the change in dye molecule concentration after adding zinc oxide nanoparticles. A 2 mL sample was collected and examined using a UV–visible spectrophotometer after every 1 hour of reaction time. Congo red had a λ_{max} at 510 nm. The absorbance of dye was used to determine the concentration of leftover dye after the photocatalytic experiment. The photocatalytic degradation efficiency (% E) of ZnO NPs was calculated using equation (3).

$$\% E = \frac{A_0 - A_t}{A_0} x100 \quad \ldots\ldots\ldots\ldots\ldots\ldots (3)$$

Where A_0 and A_t denote absorbance of dye at times t = 0 and t = t, respectively.

Bima Journal of Science and Technology, Vol. 6 (3) Dec, 2022 ISSN: 2536-6041

DOI: 10.56892/bima.v6i03.47

Table 1: Effect of catalyst loading on dye degradation

S/N	60 (min)	% E	120 (min)	% E	180 (min)	% E	240 (min)	% E	300 (min)	% E
1	1 mg	9.09	1 mg	15.58	1 mg	19.48	1 mg	20.78	1 mg	22.08
2	2 mg	15.58	2 mg	19.48	2 mg	22.08	2 mg	23.38	2 mg	25.97
3	3 mg	18.18	3 mg	23.38	3 mg	24.68	3 mg	25.97	3 mg	28.57

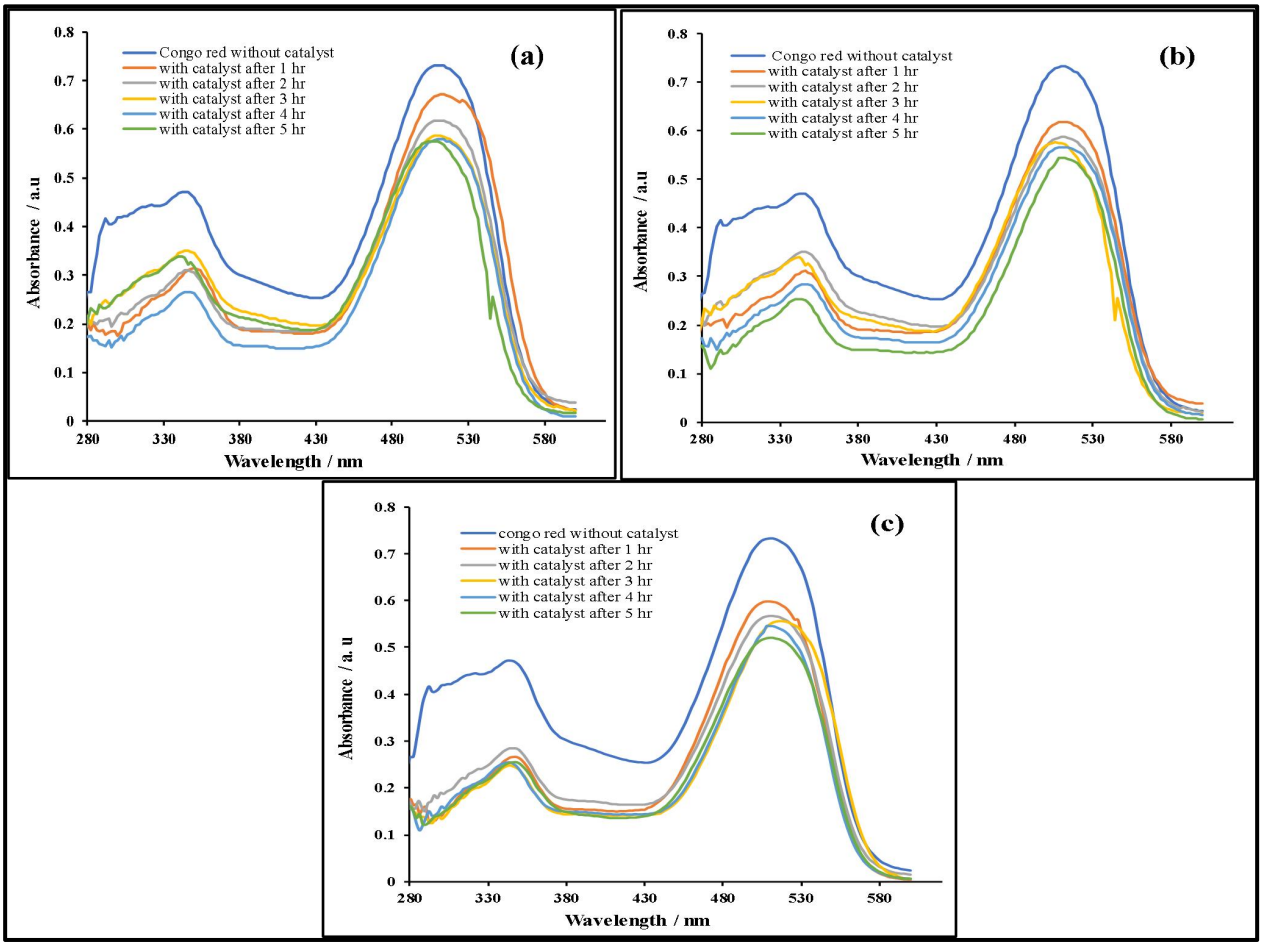

Figure 5: Plots of time dependent decrease in the absorption band intensity of the dye at (a) 1 mg, (b) 2 mg and (c) 3 mg

At 510 nm, the degradation of Congo red dye was observed after adding ZnO NPs to the dye and exposing it to solar radiation, a time-dependent drop in the dye's absorption band intensity was observed (Figure 5(a), (b), and (c)). After 5 hours, the computed degradation efficiency of Congo red dye was 22.08 %, 25.97 % and 28.57 %, respectively, for 1 mg, 2 mg, and 3 mg, suggesting that the catalyst's degradation effectiveness improves with time and catalyst loading, as shown in Table 1.

The following paragraphs provide a potential process for the photocatalytic breakdown of Congo red dye by the ZnO NP (Singh, Kumar, Kim, & Rawat, 2019).

$ZnO + h\nu \rightarrow ZnO\ (e^- + h^+)$ …….. (4)

$ZnO + h\nu \rightarrow ZnO(e^-) + ZnO(h^+)$ ……(5)

DOI: 10.56892/bima.v6i03.47

$ZnO(e^-) + O_2 \rightarrow O_2$..... (6)

$ZnO(h^+) + H_2O \rightarrow OH^-$..... (7)

O_2^- or OH^- + Dye → degraded product

ZnO nanoparticles' contact with light produced electrons and holes, which were then used in a photochemical reaction (eq. 4). While photogenerated holes oxidise the water to form hydroxyl radicals OH•, photogenerated electrons in the conduction band react with molecular oxygen (O_2). Reactive oxygen species (ROS), such as hydroxyl radicals ($\bullet OH^-$) and superoxide anions ($\bullet O_2^-$), are created because of this process (eq. 5 & eq. 6). The breakdown of dye molecules is brought on by these ROS.

Apparent Kinetic Rate Constant (k_{app})

The dye degradation kinetics was computed using Langmuir–Hinshelwood (L-H) rate equations (eq. 8) to explain the reaction's performance. This is one of the best models for elucidating the kinetic behavior of heterogeneous photocatalyst (Nezamzadeh-Ejhieh & Ghanbari-Mobarakeh, 2015).

$$r = -\frac{dc}{dt} = k\theta = k\left(\frac{KC}{1+C}\right) \quad \text{..... (8)}$$

Where r, K, C, k, c, and t represent the rate of reaction (mg L^{-1} min^{-1}), adsorption rate constant (L^- mg^{-1}, Langmuir constant related to the energy of adsorption), dye solution concentration (mg L^{-1}), photocatalysis rate constant (mg L^{-1} min^{-1}), dye solution concentration at any time, and time (min), respectively. When $KC \gg 1$, the reaction rate becomes concentration independent, i.e., r = ko, resulting in zero-order kinetics (ko = zero order rate constant). For $KC \ll 1$, on the other hand (e.g., in case of dilute sample), the rate of reaction varies linearly or proportionately with concentration (i.e., $r = -dc/dt = kKC = k_1 C$ *or* $\ln C_t/C_o = -k_1 t$).

As a result, the response is governed by the first order rate law, with k_1 being the first order rate constant. By displaying the decrease in dye concentrations (C_t/C_o) as a function of time, the rate constant may be derived. A pseudo-first order logarithmic fit was used to produce apparent rate constants (K_{app}) for the dye degradation. An K_{app} value of 8.8 x 10^{-2} min^{-1}, 6.6 x 10^{-2} min^{-1}, and 5.7 x 10^{-2} min^{-1} was estimated for 1 mg, 2 mg, and 3 mg catalyst loading, respectively (Figure 6(a), (b), and (c)), indicating that the rate of reaction increases with increasing catalyst loading.

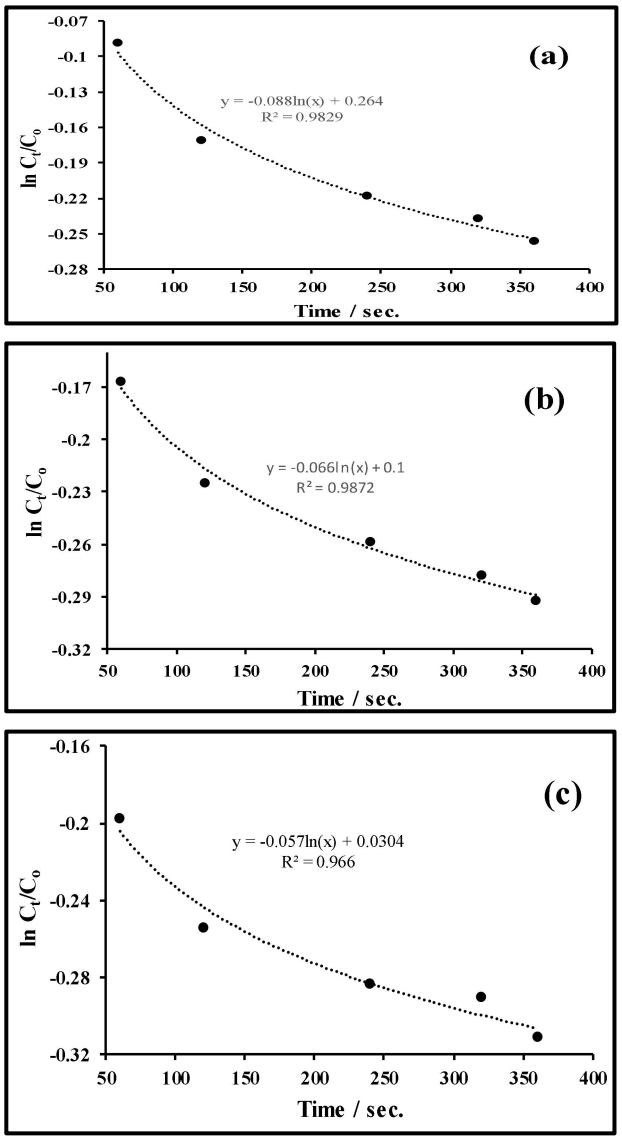

DOI: 10.56892/bima.v6i03.47

Figure 6: The line-weaver Burk plots for the degradation of Congo red dye in the presence of sunlight

CONCLUSION

Mangifera indica aqueous leaf extract was used to successfully synthesize zinc oxide nanoparticles. Color change, UV-visible spectroscopy, FTIR spectroscopy, X-ray diffraction, and scanning electron microscopy were used to establish the nanoparticle's formation. The nanoparticles absorb light at 292 nm, according to UV-visible spectroscopy, while the scanning electron microscope indicates the shape of the particles as flat sheets and strongly agglomerated, with an X-ray diffraction size of 51.53 nm. FTIR spectroscopy reveals functional groups of alcohol, amides, alkanes, amines, ethers Ar-O-R, and alkenes as potential groups responsible for the reduction of metal salt to metal oxide nanoparticles. The photocatalytic performance of the nanoparticles in the degradation of Congo red dye improves as the catalyst loading increases, with the apparent kinetic rate constants of 8.8 x 10^{-2} min^{-1}, 6.6 x 10^{-2} min^{-1}, and 5.7 x 10^{-2} min^{-1} for 1 mg, 2 mg, and 3 mg, respectively, indicating that the nanoparticle has potential in the degradation of Congo red dye.

REFERENCES

Ghidan, A., Al-Antary, T., & Awwad, A. (2016). Green synthesis of copper oxide nanoparticles using Punica granatum peels extract: effect on green peach Aphid. *Environmental Nanotechnology, Monitoring and Management* , 95-98.

Kumar, V., Mahajan, R., Kaur, I., & Kim, K. (2017). Simple and mediator-free urea sensing based on engineered nanodiamonds with polyaniline nanofibers synthesized in situ. *ACS Applied Material Interfaces*, 16813–16823.

Lu, Y., Mei, Y., Schrinner, M., Ballauf, M., Moller, M., & Breu, J. (2007). In situ formation of Ag nanoparticles in spherical polyacrylic acid brushes by UV-irradiation. *Journal of Physical Chemistry C*, 7676-7681.

Lyon, J. L., Fleming, D., Stone, M., Schiffer, P., & Williams, M. (2004). Synthesis of Fe oxide core/Au shell nanoparticles by iterative hydroxylamine seeding. *Nano Letters*, 719-723.

Mamuru, S. A., & Jaji, N. (2015). Voltammetric and impedimetric behaviour of phytosynthesized nickel nanoparticles. *Journal of nanostructures in chemistry*, 347-356.

Nezamzadeh-Ejhieh, A., & Ghanbari-Mobarakeh, Z. (2015). Heterogeneous photodegradation of 2,4-dichlorophenol using FeO doped onto nano-particles of zeolite P. *Journal of Industrial and Engineering Chemistry*, 668-676.

Ramesh, M., Anbuvannan, M., & Viruthagiri, G. (2015). Green Synthesis of ZnO Nanoparticles Using Solanum nigrum Leaf Extract and Their Antibacterial Activity. *Spectrochimica Acta Part A*, 864-870.

Roduner, E. (2006). Size Matters: Why Nanomaterials Are Different. *Chemical Society Reviews*, 583-592.

Singh, J., Kumar, V., Kim, K.-H., & Rawat, M. (2019). Biogenic synthesis of copper oxide nanoparticles using plant extract and its prodigious potential for photocatalytic degradation of dyes. *Environmental Research*, 1-12.

Sivaraj, R., Rahman, P., Rajiv, P., Salam, H., & Venckatesh, R. (2014). Biogenic copper oxide nanoparticles synthesis using Tabernaemontana divaricate leaf extract and its antibacterial activity against urinary tract pathogen. *Spectrochimica Acta Part A Molecule Biomolecule Spectroscopy*, 178–181.